

A ONE-DIMENSIONAL COARSE PRECONDITIONER FOR THREE-DIMENSIONAL UNSTEADY INCOMPRESSIBLE NAVIER-STOKES FLOWS IN PATIENT-SPECIFIC ARTERIES*

YINGZHI LIU[†], FENFEN QI[†], AND XIAO-CHUAN CAI^{†‡}

Abstract. Numerical simulation of blood flows in patient-specific arteries is becoming an important tool in understanding vascular diseases and surgery planning. Depending on the branching geometry and the patient parameters, the flow can be quite complicated with local vortex structures and rotations, but the principal component of the flow is always along the centerline of the artery. Based on this observation, we introduce a new two-level domain decomposition method for unsteady incompressible Navier-Stokes equations in three-dimensional complex patient-specific arteries, and the key component of the preconditioner is a parameterized one-dimensional unsteady Navier-Stokes or Stokes coarse problem defined along the centerline of the artery. The one-dimensional preconditioner and some overlapping three-dimensional subdomain preconditioners are combined additively to form the two-level method via interpolations using radial basis functions. The most important feature of the method is that the cost of solving the coarse problem is nearly neglectable compared with the subdomain solver. The blood flow is modeled by the unsteady incompressible Navier-Stokes equations with resistance outflow boundary conditions discretized by a stabilized finite element method on fully unstructured meshes and the second-order backward differentiation formula in time. Numerical experiments indicate that the proposed method is highly effective and robust for complex arteries with many branches, in other words, the numbers of linear and nonlinear iterations change very little when the mesh is refined or the number of subdomains is increased or the number of arterial branches is increased.

Key words. Unsteady incompressible Navier-Stokes problem with resistance boundary conditions, blood flows in artery, two-level Schwarz method, parameterized one-dimensional coarse problem, fully implicit finite element method

AMS subject classifications. 76D07, 65N30, 65N55, 65Y05

1. Introduction. Early identification can often reduce the probability of the morbidity and mortality of vascular diseases such as peripheral artery disease [43], cerebral aneurysm [25] and coronary artery atherosclerosis [8]. Hemodynamics analysis [1, 15, 44, 55, 60], the study of the behavior of blood flows, can be helpful to gain insight into the formation and progression of vascular diseases, even identify early as well as make a treatment plan for certain vascular diseases. Many clinical techniques are available for the diagnosis of vascular diseases such as computed tomography, magnetic resonance imaging, transcranial Doppler and four-dimensional flow magnetic resonance imaging. Recently with the advances in supercomputing and parallel algorithms, tremendous progress has been made on image-based computational fluid dynamics (CFD) methods to study hemodynamics because they are non-invasive and can offer reasonably accurate solutions for clinical applications [41, 45, 46, 47, 50, 59]. When simulating blood flows using image-based CFD methods, the unsteady incompressible Navier-Stokes equations are often considered with suitable outflow boundary conditions such as the resistance boundary condition and the impedance boundary condition [45, 62]. Taking account of the nonlinearity of the system and the geometrical complexity, the unsteady incompressible Navier-Stokes equations are quite difficult to solve. Many numerical methods have been developed to solve the equations discretized implicitly on fully unstructured meshes. Newton-Krylov methods [35] solve the nonlinear systems by inexact Newton methods in which the Jacobian systems are solved by a Krylov subspace method with suitable preconditioner, for example, block preconditioners [10, 11, 14, 32, 33], multigrid preconditioners [36] and overlapping Schwarz preconditioners (NKS) [3, 5]. Projection methods [26, 48, 49] split the discretized problem into some smaller problems involving the velocity and pressure fields and then approximately solve them successively. We also mention that there are many other methods for the hemodynamics simulation including lattice Boltzmann methods [51], dual-primal FETI methods [2], BDDC methods [40], multigrid methods [21] and isogeometric methods [63]. Taking advantage of Newton methods [9], Krylov subspace methods [54] and domain decomposition methods [61], in this paper, we solve the unsteady incompressible Navier-Stokes equations in patient-specific arteries by NKS and focus on the construction of a two-level additive Schwarz preconditioner with a highly effective, robust, and low cost coarse preconditioner.

*Submitted to the editors DATE.

Funding: This work was supported in part by FDCT 0141/2020/A3, 0079/2021/AFJ, and NSFC 12201658.

[†]Department of Mathematics, University of Macau, Macau, P. R. China (yingzhiliu@um.edu.mo, yc27956@umac.mo, xc-cai@um.edu.mo).

[‡]Corresponding author.

48 In two-level additive Schwarz preconditioners, the coarse problem together with its restriction and
 49 extension plays a crucial role in the overall performance. In [27, 28], a monolithic overlapping Schwarz pre-
 50 conditioner with generalized Dryja-Smith-Widlund (GDSW) coarse spaces was introduced and studied, the
 51 method was inspired by the original GDSW coarse spaces [12] and the monolithic Schwarz preconditioner
 52 [34]. [37, 38] introduced a coarse problem by discretizing the original problem in a geometry-preserving
 53 three-dimensional coarse mesh. Since the geometries of the coarse and fine meshes match each other, the re-
 54 striction and extension matrices can be constructed by the finite element basis functions of the coarse mesh.
 55 [7] presented a non-nested coarse mesh to reduce the number of mesh points of the geometry-preserving
 56 coarse mesh near the wall and the restriction and extension matrices are defined using radial basis functions
 57 to deal with the non-matching geometries of the coarse and fine meshes. All the coarse meshes developed
 58 in [7, 37, 38] are three-dimensional and solving these coarse problems takes a significant percentage of the
 59 overall compute time.

60 Recently, for steady Stokes equations in two-dimensional tube-like domains, we introduced a coarse
 61 problem based on the parameterized one-dimensional steady Stokes equations defined on the centerline of
 62 the domain, and showed that the method is quite effective to reduce the number of iterations and the cost of
 63 the coarse preconditioner is nearly negligible [42]. In fact, as cheap approximations of complex blood flows
 64 in three-dimensional arteries, one-dimensional models have been studied widely [17, 18, 56, 58]. However,
 65 limited by the characteristics of one-dimensional models, most of the studies focus on the global behaviors
 66 of the flow such as the averaged pressure and the flow waveforms [52, 53] or combining the one-dimensional
 67 model with three-dimensional models to simulate blood flows in multiscale arteries [16]. In this paper, we
 68 extend the idea of the one-dimensional coarse preconditioner to a one-dimensional unsteady Navier-Stokes
 69 model to solve the unsteady incompressible Navier-Stokes equations in three-dimensional patient-specific
 70 arteries. The full three-dimensional Navier-Stokes model is sometimes necessary especially for exploring the
 71 localized hemodynamic quantities such as the wall shear stress, local vortex dynamics, and flow rotations in
 72 patient-specific arteries [24, 55].

73 The one-dimensional model of the unsteady incompressible Navier-Stokes equations on the centerline of
 74 an artery with multiple branches is obtained by a homogenization of the three-dimensional unsteady incom-
 75 pressible Navier-Stokes model on the cross section with suitable compatibility conditions at bifurcations. We
 76 then use a fully discretized matrix of the one-dimensional model to construct the one-dimensional coarse
 77 preconditioner with appropriate restriction and extension matrices between the one-dimensional coarse mesh
 78 and the three-dimensional fine mesh. Experiments show that the method works quite well even for situations
 79 with a large number of branches. It is known that in a cardiac cycle, the flow is usually easier to model in
 80 the diastole phase than the systole phase, and the proposed method works well in both phases. This type of
 81 robustness is important for clinical applications.

82 The rest of the paper is organized as follows. In Section 2 we describe the model problem and the
 83 stabilized finite element discretization. In Section 3 we briefly recall the Newton-Krylov-Schwarz method
 84 and focus on the details of the one-dimensional coarse preconditioner. Section 4 shows some numerical
 85 experiments for patient-specific arteries to verify the effectiveness and robustness of the one-dimensional
 86 coarse preconditioner. Some concluding remarks are given in Section 5.

87 **2. Unsteady incompressible Navier-Stokes model with resistance outflow boundary condi-**
 88 **tion and its stabilized finite element discretization.** Consider the unsteady incompressible Navier-
 89 Stokes problem in an arterial domain $\Omega \in \mathbb{R}^3$ (see Fig. 1),

$$90 \quad (2.1) \quad \begin{cases} \rho \left(\frac{\partial \mathbf{u}}{\partial t} + \mathbf{u} \cdot \nabla \mathbf{u} \right) - \nu \Delta \mathbf{u} + \nabla p = \mathbf{f} & \text{in } \Omega \times (0, T), \\ \nabla \cdot \mathbf{u} = \mathbf{0} & \text{in } \Omega \times (0, T), \\ \mathbf{u}(\mathbf{x}, 0) = \mathbf{u}_0(\mathbf{x}) & \text{in } \Omega, \end{cases}$$

91 where \mathbf{u} and p are the velocity and pressure, \mathbf{f} and \mathbf{u}_0 are the given source term and initial velocity, ρ
 92 and ν are the blood density and viscosity coefficient. Denote by $\partial\Omega = \Gamma_I \cup \Gamma_W \cup \Gamma_O$ the boundary of the
 93 domain, where Γ_I , Γ_W and $\Gamma_O = \bigcup_{i=1}^m \Gamma_O^i$ are the inlet boundary, the arterial wall and the m outlet boundaries,
 94 respectively. On the boundaries, we impose a Dirichlet condition for the inlet velocity, a no-slip condition
 95 on the wall velocity, and a resistance condition on the outlet pressure; more precisely, we have the following

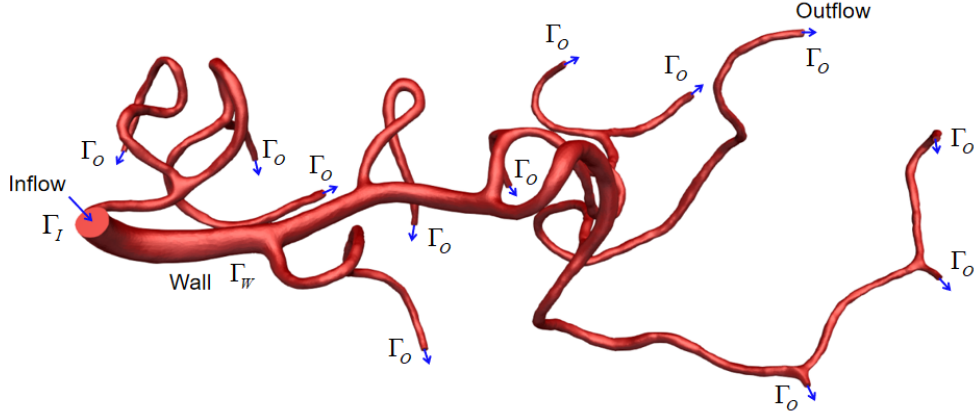


Fig. 1: A sample artery with 1 inlet and 12 outlets

96 conditions:

97 (2.2) $\mathbf{u} = \mathbf{u}_I$ on $\Gamma_I \times (0, T)$,

98 (2.3) $\mathbf{u} = 0$ on $\Gamma_W \times (0, T)$,

100 (2.4) $p = R_i Q_i$ on $\Gamma_O^i \times (0, T)$,

101 where \mathbf{u}_I is the inlet velocity, R_i is the constant resistance and $Q_i = \int_{\Gamma_O^i} \mathbf{u} \cdot \mathbf{n} d\Gamma_O^i$ is the fluid flux at the
 102 local outlet surface Γ_O^i with the outward unit normal vector \mathbf{n} .

103 Before introducing the weak form of (2.1), we define $\mathbf{H}_W^1(\Omega) = \{\mathbf{v} \in \mathbf{H}^1(\Omega) : \mathbf{v}|_{\Gamma_I} = \mathbf{u}_I, \mathbf{v}|_{\Gamma_W} = 0\}$,
 104 $\mathbf{H}_{IW}^1(\Omega) = \{\mathbf{v} \in \mathbf{H}^1(\Omega) : \mathbf{v}|_{\Gamma_I \cup \Gamma_W} = 0\}$. Then the variational formulation of (2.1) with boundary conditions
 105 (2.2)–(2.4) is to find $(\mathbf{u}(\cdot, t), p(\cdot, t)) \in \mathbf{H}_W^1(\Omega) \times L^2(\Omega)$ such that

106
$$\left(\rho \frac{\partial \mathbf{u}}{\partial t}, \mathbf{v} \right) + (\nu \nabla \mathbf{u}, \nabla \mathbf{v}) - (p, \nabla \cdot \mathbf{v}) + (q, \nabla \cdot \mathbf{u}) + (\rho \mathbf{u} \cdot \nabla \mathbf{u}, \mathbf{v})$$

107 (2.5)
$$- \langle \nu \nabla \mathbf{u} \cdot \mathbf{n}, \mathbf{v} \rangle_{\Gamma_O} + \sum_{i=1}^m R_i \int_{\Gamma_O^i} \mathbf{u} \cdot \mathbf{n} d\Gamma_O^i \int_{\Gamma_O^i} \mathbf{v} \cdot \mathbf{n} d\Gamma_O^i = (\mathbf{f}, \mathbf{v}),$$

108

109 for all $(\mathbf{v}, q) \in \mathbf{H}_{IW}^1(\Omega) \times L^2(\Omega)$ and $t \in (0, T)$, where $(u, v) := \int_{\Omega} uv d\Omega$ and $\langle u, v \rangle_{\Gamma} := \int_{\Gamma} uv d\Gamma$.

110 Let \mathcal{T}_h be a shape-regular unstructured tetrahedral mesh of Ω , and the continuous, piecewise linear
 111 polynomial function space on \mathcal{T}_h is denoted by S_h . We define the finite element spaces $\mathbf{V}_h = [S_h]^3 \cap \mathbf{H}_W^1(\Omega)$,
 112 $\mathbf{W}_h = [S_h]^3 \cap \mathbf{H}_{IW}^1(\Omega)$ for the velocity and $Q_h = S_h \cap L^2(\Omega)$ for the pressure. Considering the advantages
 113 of the low- and equal-order finite element pair in terms of the computational complexity and the ease of
 114 implementation compared with the stable finite element pairs, following [7, 19], we use the stabilized finite
 115 element method to spatially discretize the weak formulation (2.5), that is, to find $(\mathbf{u}_h(\cdot, t), p_h(\cdot, t)) \in \mathbf{V}_h \times Q_h$,

116 such that

$$\begin{aligned}
 117 \quad (2.6) \quad & \left\{ \begin{aligned}
 & \left(\rho \frac{\partial \mathbf{u}_h}{\partial t}, \mathbf{v}_h \right) + (\nu \nabla \mathbf{u}_h, \nabla \mathbf{v}_h) - (p_h, \nabla \cdot \mathbf{v}_h) + (q_h, \nabla \cdot \mathbf{u}_h) + (\rho \mathbf{u}_h \cdot \nabla \mathbf{u}_h, \mathbf{v}_h) \\
 & - \langle \nu \nabla \mathbf{u}_h \cdot \mathbf{n}, \mathbf{v}_h \rangle_{\Gamma_O} + \sum_{i=1}^m R_i \int_{\Gamma_O^i} \mathbf{u}_h \cdot \mathbf{n} d\Gamma_O^i \int_{\Gamma_O^i} \mathbf{v}_h \cdot \mathbf{n} d\Gamma_O^i \\
 & + \sum_{K \in \mathcal{T}_h} \left(\rho \left(\frac{\partial \mathbf{u}_h}{\partial t} + \mathbf{u}_h \cdot \nabla \mathbf{u}_h \right) + \nabla p_h, \gamma_1 (\mathbf{u}_h \cdot \nabla \mathbf{v}_h + \nabla q_h) \right)_K \\
 & + \sum_{K \in \mathcal{T}_h} (\nabla \cdot \mathbf{u}_h, \gamma_2 \nabla \cdot \mathbf{v}_h)_K \\
 & = (\mathbf{f}, \mathbf{v}_h) + \sum_{K \in \mathcal{T}_h} (\mathbf{f}, \gamma_1 (\mathbf{u}_h \cdot \nabla \mathbf{v}_h + \nabla q_h))_K,
 \end{aligned} \right.
 \end{aligned}$$

118 for all $(\mathbf{v}_h, q_h) \in \mathbf{W}_h \times Q_h$ and $t \in (0, T)$. Here the stabilization parameters γ_1 and γ_2 are defined as

$$119 \quad \gamma_1 = \left(\sqrt{\frac{4}{\Delta t^2} + \mathbf{u}_h^T \mathbf{G} \mathbf{u}_h + 36 \left(\frac{\nu}{\rho} \right)^2 \mathbf{G} : \mathbf{G}} \right)^{-1}, \quad \gamma_2 = \left(8\gamma_1 \sum_{i=1}^3 G_{i,i} \right)^{-1},$$

120 where $\mathbf{G} = (G_{i,j})$, $(i, j = 1, 2, 3)$ is the covariant metric tensor satisfying $G_{i,j} = \sum_{k=1}^3 \frac{\partial \hat{x}_k}{\partial x_i} \frac{\partial \hat{x}_k}{\partial x_j}$, $\{\hat{x}_i\}_{i=1}^3$ and

121 $\{x_i\}_{i=1}^3$ are the local reference and global physical coordinate variables, respectively. Let $\{\varphi_i\}_{i=1}^N$ be the basis

122 functions, where N is the number of mesh points. Then the numerical solution \mathbf{u}_h and p_h can be written as

123 $\mathbf{u}_h(t, x) = \sum_{i=1}^N (U_i(t), V_i(t), W_i(t)) \varphi_i(x)$ and $p_h(t, x) = \sum_{i=1}^N P_i(t) \varphi_i(x)$, where $U = (U_i)$, $V = (V_i)$, $W = (W_i)$

124 and $P = (P_i)$ are the vector of the nodal values of the velocity unknowns and the pressure unknowns, respectively. Define $X = (U, V, W, P)^T$ and then (2.6) can be rewritten as a system of ordinary differential

125 equations

$$127 \quad (2.7) \quad \frac{dX}{dt} = L(X).$$

128 Considering the numerical accuracy, instead of the implicit backward Euler formula, we use the second-order

129 backward differentiation formula (BDF2) for the temporal discretization with the time step size Δt , then

130 the fully discretized system at $t = n\Delta t$ is given by

$$131 \quad (2.8) \quad \frac{\frac{3}{2}X^n - 2X^{n-1} + \frac{1}{2}X^{n-2}}{\Delta t} = L(X^n), \quad (n \geq 2)$$

132 where X^1 can be obtained by the first-order implicit Euler method with the given initial value X^0 .

133 3. Implicit solver with a two-level Schwarz preconditioner.

134 The nonlinear algebraic system (2.8)

135 is large, sparse, and quite difficult to solve because its underlying arterial geometry is complex and its solution

136 involves highly nonlinear features. In a cardiac cycle, many systems of form (2.8) need to be constructed

137 and solved, and some of them are relatively easy to solve but others are difficult to solve, therefore a robust

138 nonlinear solver is important for the simulation of the blood flow in a whole cardiac cycle. Rewrite the

139 nonlinear system (2.8) as

$$139 \quad (3.1) \quad F^n(X^n) = 0.$$

140 The general framework of the nonlinear solver [5] can be described as follows.

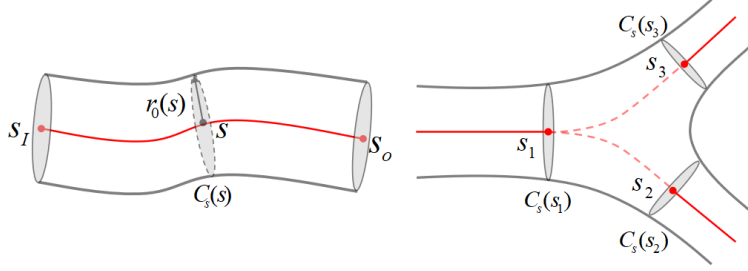


Fig. 2: A non-bifurcating (left) and a bifurcating (right) artery with the marked centerline and cross sections.

Algorithm 3.1 Inexact Newton for $F^n(X^n) = 0$

- 1: Give an initial guess $X_0^n = X^{n-1}$.
- 2: **for** $k = 0, 1, 2, \dots$ **do**
- 3: Find the Newton direction s_k^n by solving the Jacobian system by a preconditioned restarted GMRES method

$$(3.2) \quad J_k^n (M_k^n)^{-1} M_k^n s_k^n = -F^n(X_k^n),$$

with the stopping criterion

$$(3.3) \quad \|F^n(X_k^n) + J_k^n s_k^n\|_2 \leq \max \{atol_{\text{GMRES}}, rtol_{\text{GMRES}} \|F^n(X_k^n)\|_2\}.$$

- 4: Find the step size λ_k^n by the line search technique (Armijo rule)

$$(3.4) \quad f(X_k^n + \lambda_k^n s_k^n) \leq f(X_k^n) + \varepsilon \lambda_k^n \nabla f(X_k^n)^T s_k^n.$$

- 5: Update the Newton solution $X_{k+1}^n = X_k^n + \lambda_k^n s_k^n$.
 - 6: **if** $\|F^n(X_{k+1}^n)\|_2 < \max \{atol_{\text{Newton}}, rtol_{\text{Newton}} \|F^n(X_0^n)\|_2\}$ **then**
 - 7: $X^n = X_{k+1}^n$, return.
 - 8: **end if**
 - 9: **end for**
-

141 In Algorithm 3.1, J_k^n is the analytically constructed Jacobian matrix of the nonlinear system F^n at
 142 X_k^n , $(M_k^n)^{-1}$ is a preconditioner to be discussed later, f is a merit function defined as $f(X) = \|F(X)\|_2^2/2$
 143 and ε is a control parameter with a default value $\varepsilon = 10^{-4}$. The user-defined absolute and relative tolerances
 144 $atol_{\text{GMRES}}, rtol_{\text{GMRES}}$ and $atol_{\text{Newton}}, rtol_{\text{Newton}}$ are used to control the Krylov and Newton iterations,
 145 respectively.

146 In order to construct an efficient preconditioner M_k^n at each Newton step, we consider a two-level over-
 147 lapping additive Schwarz preconditioner of the form $M^{-1} = M_{cl}^{-1} + M_{1s}^{-1}$, where M_{cl}^{-1} is a one-dimensional
 148 coarse preconditioner and M_{1s}^{-1} is the sum of some three-dimensional subdomain preconditioners, which will
 149 be introduced in the following subsections.

150 **3.1. One-dimensional coarse preconditioner.** We consider a coarse preconditioner of the form

$$151 \quad (3.5) \quad M_{cl}^{-1} = E_{cl} A_{cl}^{-1} R_{cl},$$

152 where A_{cl} is the discretized matrix of a coarse problem, R_{cl} and E_{cl} are the restriction and extension
 153 matrices between the coarse and fine finite element spaces, respectively. In this subsection, we focus on
 154 the construction of a coarse preconditioner in which A_{cl} is derived from discretizing a parameterized one-
 155 dimensional unsteady Navier-Stokes coarse problem defined on the centerline of the artery. The problem
 156 is obtained by an approximate integration of the three-dimensional Navier-Stokes equations on the cross
 157 section centered at a point on the centerline.

158 **3.1.1. One-dimensional parameterized unsteady incompressible Navier-Stokes equations**
 159 **and their discretization.** Denote Ω_{cl} as the centerline of Ω , which is a curve in the three-dimensional

160 space parameterized by the arc length s , $C_s(s)$ as the cross section of Ω and $A_s(s)$ as the corresponding area.
 161 Let $u^{cl}(t, s)$ be the tangential component of the velocity along the centerline and $p^{cl}(t, s)$ be the value of the
 162 pressure on the centerline. We assume that the pressure is a constant on each cross section and the velocity
 163 consists mainly of the component u_s along the centerline, i.e., $\mathbf{u} \approx u_s \boldsymbol{\tau}$, where $\boldsymbol{\tau} = (\tau^1, \tau^2, \tau^3)$ is the unit
 164 tangent vector along the centerline. Further we assume that the component u_s has a parabolic profile at
 165 each cross section, i.e.,

$$166 \quad (3.6) \quad u_s(t, r, s) = u^{cl}(t, s) \zeta \left(\frac{r}{r_0(s)} \right),$$

167 where $\zeta(y) = (1 - y^2)$ ($y \in [0, 1]$) is a parabolic profile function, $r_0(s)$ is the radius of $C_s(s)$ and r is the
 168 radial coordinate with respect to $C_s(s)$. Define $Q = \int_{C_s} u_s dC_s$ as the flux on the cross section C_s . For
 169 a non-bifurcating artery Ω (see the left sub-figure in Fig. 2), the one-dimensional unsteady Navier-Stokes
 170 model on the centerline Ω_{cl} can be described as [42, 46]

$$171 \quad (3.7) \quad \begin{cases} \rho \frac{\partial Q}{\partial t} + \beta \rho \alpha \frac{\partial}{\partial s} \left(\frac{Q^2}{A_s} \right) + K_r \frac{Q}{A_s} + A_s \frac{\partial p^{cl}}{\partial s} = f^{cl}, \\ \frac{\partial Q}{\partial s} = 0, \quad u^{cl}(s, 0) = u_0^{cl}(s), \end{cases}$$

172 where $\alpha = 4/3$ is the Coriolis coefficient, $K_r = 8\pi\nu$, $f^{cl} = \int_{C_s} \mathbf{f} \cdot \boldsymbol{\tau} dC_s$ and $u_0^{cl} = \int_{C_s} \mathbf{u}_0 \cdot \boldsymbol{\tau} dC_s$. Here $\beta = 0$
 173 represents the one-dimensional Stokes model and $\beta = 1$ represents the Navier-Stokes model. By the flux
 174 conservation equation $\frac{\partial Q}{\partial s} = 0$, the nonlinear term $\frac{\partial}{\partial s} \left(\frac{Q^2}{A_s} \right)$ in (3.7) can be reduced as $Q \frac{\partial}{\partial s} \left(\frac{Q}{A_s} \right)$. Based
 175 on the assumption (3.6), we have $Q = A_s u^{cl}/2$, and (3.7) can be rewritten as

$$176 \quad (3.8) \quad \begin{cases} \rho \frac{A_s}{2} \frac{\partial u^{cl}}{\partial t} + \beta \rho \frac{\alpha}{4} A_s u^{cl} \frac{\partial u^{cl}}{\partial s} + \frac{K_r}{2} u^{cl} + A_s \frac{\partial p^{cl}}{\partial s} = f^{cl}, \\ \frac{\partial (A_s u^{cl})}{\partial s} = 0, \quad u^{cl}(s, 0) = u_0^{cl}(s). \end{cases}$$

177 At the inlet point s_I and the outlet point s_o of the centerline, we consider the following boundary conditions

$$178 \quad (3.9) \quad u^{cl}(s_I, t) = -\frac{2}{|\Gamma_I|} \int_{\Gamma_I} \mathbf{u}_I \cdot \mathbf{n} d\Gamma_I := u_I^{cl},$$

$$179 \quad (3.10) \quad p^{cl}(s_o, t) = R_o Q_o \approx \frac{R_o A_s(s_o)}{2} u^{cl}(s_o, t),$$

181 obtained by integrating (2.2) on the inlet boundary and (2.4) on the outlet boundary.

182 Define the centerline velocity function spaces $M(\Omega_{cl}) = \{v^{cl} \in H^1(\Omega_{cl}) : v^{cl}(s_I) = u_I^{cl}\}$, $M_0(\Omega_{cl}) =$
 183 $\{v^{cl} \in H^1(\Omega_{cl}) : v^{cl}(s_I) = 0, v^{cl}(s_o) = 0\}$. Then the variational formulation of the one-dimensional prob-
 184 lem (3.8) with the boundary conditions (3.9)–(3.10) is to find $(u^{cl}(\cdot, t), p^{cl}(\cdot, t)) \in M(\Omega_{cl}) \times L^2(\Omega_{cl})$ such
 185 that

$$186 \quad (3.11) \quad \begin{cases} \left(\rho \frac{A_s}{2} \frac{\partial u^{cl}}{\partial t}, v^{cl} \right) + \beta \left(\rho \frac{\alpha}{4} A_s u^{cl} \frac{\partial u^{cl}}{\partial s}, v^{cl} \right) + \left(\frac{K_r}{2} u^{cl}, v^{cl} \right) \\ + A_s v^{cl} p^{cl} \Big|_{s_I}^{s_o} - \left(\frac{\partial (A_s v^{cl})}{\partial s}, p^{cl} \right) + \left(\frac{\partial (A_s u^{cl})}{\partial s}, q^{cl} \right) = (f^{cl}, v^{cl}), \\ \frac{R_o A_s(s_o)}{2} u^{cl}(s_o) - p^{cl}(s_o) = 0, \end{cases}$$

187 for all $(v^{cl}, q^{cl}) \in M_0(\Omega_{cl}) \times L^2(\Omega_{cl})$ and $t \in (0, T)$. Let \mathcal{T}_h^{cl} be a polyline mesh for Ω_{cl} with the mesh
 188 size $O(h_{cl})$ and S_h^{cl} be the corresponding continuous, piecewise linear polynomial function space. Define the
 189 finite element spaces $V_h^{cl} = S_h^{cl} \cap M(\Omega_{cl})$, $W_h^{cl} = S_h^{cl} \cap M_0(\Omega_{cl})$ for the velocity and $Q_h^{cl} = S_h^{cl} \cap L^2(\Omega_{cl})$ for

190 the pressure. The stabilized finite element discretization of the weak formulation (3.11) is written as: find
 191 $(u_h^{cl}(\cdot, t), p_h^{cl}(\cdot, t)) \in V_h^{cl} \times Q_h^{cl}$, such that

$$192 \quad (3.12) \quad \left\{ \begin{array}{l} \left(\rho \frac{A_s}{2} \frac{\partial u_h^{cl}}{\partial t}, v_h^{cl} \right) + \beta \left(\rho \frac{\alpha}{4} A_s u_h^{cl} \frac{\partial u_h^{cl}}{\partial s}, v_h^{cl} \right) + \left(\frac{K_r}{2} u_h^{cl}, v_h^{cl} \right) \\ + \left(A_s v_h^{cl}, \frac{\partial p_h^{cl}}{\partial s} \right) - \left(A_s u_h^{cl}, \frac{\partial q_h^{cl}}{\partial s} \right) + A_s u_h^{cl} q_h^{cl} \Big|_{s_I}^{s_o} \\ + \gamma_{cl} \sum_{e \in \mathcal{T}_h^{cl}} \left(\rho \frac{A_s}{2} \frac{\partial u_h^{cl}}{\partial t} + \beta \rho \frac{\alpha}{4} A_s u_h^{cl} \frac{\partial u_h^{cl}}{\partial s} + \frac{K_r}{2} u_h^{cl} + A_s \frac{\partial p_h^{cl}}{\partial s}, h_{cl}^2 \frac{\partial q_h^{cl}}{\partial s} \right)_e \\ = (f^{cl}, v_h^{cl}) + \gamma_{cl} \sum_{e \in \mathcal{T}_h^{cl}} \left(f^{cl}, h_{cl}^2 \frac{\partial q_h^{cl}}{\partial s} \right)_e, \\ \frac{R_o A_s(s_o)}{2} u_h^{cl}(s_o) - p_h^{cl}(s_o) = 0, \end{array} \right.$$

193 for all $(v_h^{cl}, q_h^{cl}) \in W_h^{cl} \times Q_h^{cl}$ and $t \in (0, T)$, where $\gamma_{cl} > 0$ is a stabilization parameter. Using the implicit
 194 first-order backward Euler method for the temporal discretization with the time step size Δt , we have a
 195 linearized and fully discretized scheme of (3.12) at $t = n\Delta t$

$$196 \quad (3.13) \quad \left\{ \begin{array}{l} \mathcal{B}_{cl} \left(u_h^{cl,n}, p_h^{cl,n}; v_h^{cl}, q_h^{cl} \right) = (F_{cl}, v_h^{cl}) + \gamma_{cl} \sum_{e \in \mathcal{T}_h^{cl}} \left(F_{cl}, h_{cl}^2 \frac{\partial q_h^{cl}}{\partial s} \right)_e, \\ \frac{R_o A_s(s_o)}{2} u_h^{cl,n}(s_o) - p_h^{cl,n}(s_o) = 0, \end{array} \right.$$

where

$$F_{cl} = f^{cl} + \rho \frac{A_s}{2\Delta t} u_h^{cl,n-1} + \beta \rho \frac{\alpha}{4} A_s u_h^{cl,n-1} \frac{\partial}{\partial s} \left(u_h^{cl,n-1} \right)$$

197 and

$$198 \quad \mathcal{B}_{cl} \left(u_h^{cl,n}, p_h^{cl,n}; v_h^{cl}, q_h^{cl} \right) = (B_{cl}, v_h^{cl}) + \gamma_{cl} \sum_{e \in \mathcal{T}_h^{cl}} \left(B_{cl}, h_{cl}^2 \frac{\partial q_h^{cl}}{\partial s} \right)_e - \left(A_s u_h^{cl,n}, \frac{\partial q_h^{cl}}{\partial s} \right) \\ 199 \quad + A_s u_h^{cl,n} q_h^{cl} \Big|_{s_I}^{s_o}, \\ 200$$

with

$$B_{cl} = \rho \frac{A_s}{2\Delta t} u_h^{cl,n} + \beta \rho \frac{\alpha}{4} A_s \left(u_h^{cl,n-1} \frac{\partial}{\partial s} \left(u_h^{cl,n} \right) + u_h^{cl,n} \frac{\partial}{\partial s} \left(u_h^{cl,n-1} \right) \right) + \frac{K_r}{2} u_h^{cl,n} + A_s \frac{\partial p_h^{cl,n}}{\partial s}.$$

201 The coarse matrix A_{cl} is simply the matrix form of (3.13). The linearized term (i.e., the second term in B_{cl})
 202 corresponds to the nonlinear term in (3.8). When $\beta = 0$, this term vanishes and the matrix A_{cl} degenerates
 203 into the one-dimensional Stokes matrix.

204 For general bifurcating arterial networks, the one-dimensional model can be derived by combining the
 205 one-dimensional model (3.8) at each non-bifurcating branch with suitable compatibility conditions on each
 206 bifurcation. To briefly describe the conditions, we assume that there is one inflow branch and two outflow
 207 branches on each bifurcation, see the right sub-figure in Fig. 2, then using the conservation of flux and the
 208 continuity of the pressure [17, 42] on each bifurcation, we have the compatibility conditions

$$209 \quad (3.14) \quad A_s(s_1) u^{cl}(s_1) = A_s(s_2) u^{cl}(s_2) + A_s(s_3) u^{cl}(s_3), \quad p^{cl}(s_1) = p^{cl}(s_2) = p^{cl}(s_3).$$

210 For more general bifurcations involving more bifurcating branches, similar compatibility conditions can also
 211 be given.

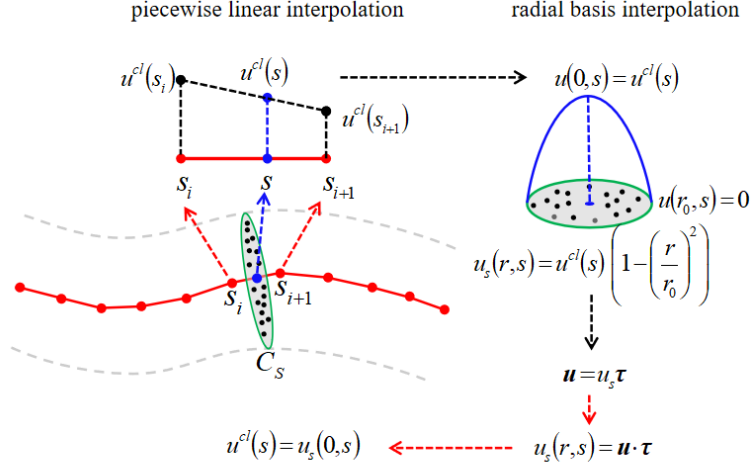


Fig. 3: Diagram of the extension process from the one-dimensional space to the three-dimensional space by piecewise linear and radial basis interpolations. First obtain the value at the point on the centerline (blue point) of the cross section (green section) by linear interpolation and then use it to obtain the value at the mesh points (black points) on the cross section by a radial basis interpolation.

212 **3.1.2. 1D-3D restriction and extension matrices.** Let $\{\mathbf{x}_i\}_{i=1}^N$ and $\{\mathbf{x}(s_i)\}_{i=1}^{N_{cl}}$ be the collection of
 213 mesh points of \mathcal{T}_h and \mathcal{T}_h^{cl} , respectively. Denote $\{I_i\}_{i=1}^{N_{cl}-1}$ as the collection of line elements of \mathcal{T}_h^{cl} . Then for
 214 any s in \mathcal{T}_h^{cl} , there exists a unique $j \in \{1, \dots, N_{cl} - 1\}$, denoted by $j(s)$, such that $s \in I_j$. Define a mapping
 215 $\mathcal{I} : \{\mathbf{x}_i\}_{i=1}^N \rightarrow \{I_i\}_{i=1}^{N_{cl}-1}$ by

$$216 \quad \mathcal{I}(\mathbf{x}_i) = I_j,$$

217 where $j = \min_{s \in s^*} j(s)$ and $s^* = \arg \min_{s \in \mathcal{T}_h^{cl}} |\mathbf{x}_i - \mathbf{x}(s)|$. We define an extension operator from $(u_h^{cl}, p_h^{cl}) \in V_h^{cl} \times Q_h^{cl}$
 218 to $(\mathbf{u}_h, p_h) \in V_h \times Q_h$ as

$$219 \quad (3.15) \quad \mathbf{u}_h(\mathbf{x}_j) = u_h^{cl}(s) \zeta \left(\frac{|\mathbf{x}_j - \mathbf{x}(s)|}{r_0(s)} \right) \boldsymbol{\tau}(s), \quad p_h(\mathbf{x}_j) = p_h^{cl}(s),$$

220 for any \mathbf{x}_j ($j = 1, \dots, N$) with s satisfying $s \in \mathcal{I}(\mathbf{x}_j)$ and $\mathbf{x}_j \in C_s(s)$. The extension operator (3.15) can
 221 be described in two steps, for a non-bifurcating artery as shown in Fig. 3: (1) first for each line segment
 222 $[s_i, s_{i+1}]$ we compute the value of the function at $s \in [s_i, s_{i+1}]$ by the piecewise linear interpolation; (2) we
 223 compute the values of the function for mesh points on the cross section $C_s(s)$ by the parabolic radial basis
 224 interpolation. For any \mathbf{x}_j , we denote by $r_j = |\mathbf{x}_j - \mathbf{x}(s)|$, where s satisfies $s \in \mathcal{I}(\mathbf{x}_j)$ and $\mathbf{x}_j \in C_s(s)$. Let
 225 the influence set D_i of s_i be defined as

$$226 \quad D_i = \left\{ \mathbf{x} \in \{\mathbf{x}_i\}_{i=1}^N : \mathcal{I}(\mathbf{x}) \subset [s_{i-1}, s_{i+1}], \mathbf{x} \in C_s(s), \forall s \in [s_{i-1}, s_{i+1}] \right\}.$$

227 Below we describe the detailed algorithm to compute the 3D-1D restriction and 1D-3D extension matrices.

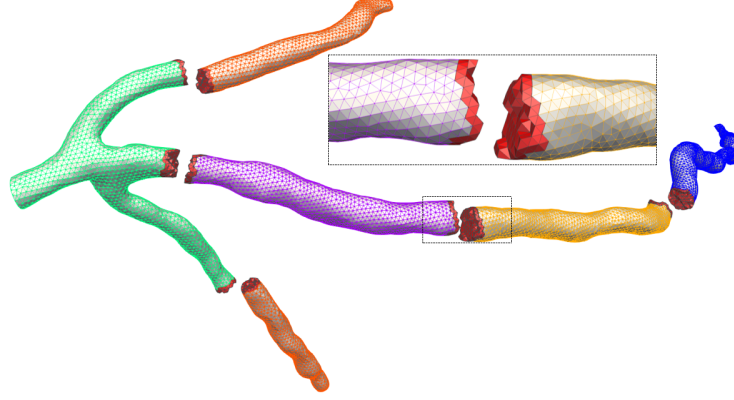


Fig. 4: Example of non-overlapping and overlapping partitions of an arterial domain with one overlapping layer, where the red elements represent the overlapping part.

Algorithm 3.2 Computation of the 3D-1D restriction matrix R_{cl} and 1D-3D extension matrix E_{cl}

- 1: Construct the $N_{cl} \times N$ weighting matrices $W^u = (w_{i,j}^u)$ for the velocity and $W^p = (w_{i,j}^p)$ for the pressure with the weighting coefficients

$$w_{i,j}^u = \begin{cases} \zeta \begin{pmatrix} r_j \\ r_0 \end{pmatrix} \phi_i(s), & \mathbf{x}_j \in D_i, \mathbf{x}_j \in C_s(s) \\ 0, & \mathbf{x}_j \notin D_i \end{cases}, \quad w_{i,j}^p = \begin{cases} \psi_i(s), & \mathbf{x}_j \in D_i, \mathbf{x}_j \in C_s(s) \\ 0, & \mathbf{x}_j \notin D_i \end{cases},$$

where $\{\phi_i\}_{i=1}^{N_{cl}}$ are the nodal basis functions of S_h^{cl} and $\psi_i(s)$ is a function of s .

- 2: Calculate the $N_{cl} \times N_{cl}$ tangent matrices T_k ($k = 1, 2, 3$) as

$$(3.16) \quad T_k := \text{diag} \left(\tau^k(s_1), \dots, \tau^k(s_{N_{cl}}) \right),$$

where $\tau^k(s_i)$ is the k th component of the unit tangent vector $\boldsymbol{\tau}$ at the mesh point s_i .

- 3: Construct the $2N_{cl} \times 4N$ restriction matrix R_{cl} by

$$(3.17) \quad R_{cl} = \begin{pmatrix} W_1^u & W_2^u & W_3^u & 0 \\ 0 & 0 & 0 & W^p \end{pmatrix}, \quad W_k^u = T_k W^u \quad (k = 1, 2, 3),$$

with $\psi_i(s) = 1$ in W^p .

- 4: Construct the $4N \times 2N_{cl}$ extension matrix E_{cl} by

$$(3.18) \quad E_{cl} = \begin{pmatrix} W_1^u & W_2^u & W_3^u & 0 \\ 0 & 0 & 0 & W^p \end{pmatrix}^T, \quad W_k^u = T_k W^u \quad (k = 1, 2, 3),$$

with $\psi_i(s) = \phi_i(s)$ in W^p .

3.2. Multiscale two-level additive Schwarz preconditioner. In this subsection, we introduce a multiscale restricted additive Schwarz preconditioner consisting of a one-dimensional coarse preconditioner and some overlapping three-dimensional subdomain preconditioners. Let us first divide the arterial domain Ω into np non-overlapping subdomains $\{\Omega_i\}_{i=1}^{np}$ such that each subdomain Ω_i consists of some elements in \mathcal{T}_h denoted by $\mathcal{T}_{h,i}$, i.e., $\mathcal{T}_h = \bigcup_{i=1}^{np} \mathcal{T}_{h,i}$, where $\mathcal{T}_{h,i} \cap \mathcal{T}_{h,j} = \emptyset$ for $i \neq j$. In practice, this step is often realized by some graph partitioning libraries such as METIS or ParMETIS [31]. Then we obtain the overlapping subdomains $\{\Omega_i^\delta\}_{i=1}^{np}$ with the mesh $\mathcal{T}_{h,i}^\delta$ by extending each subdomain Ω_i with δ layers of elements from neighboring subdomains (see Fig. 4), i.e.,

$$\mathcal{T}_{h,i}^0 = \mathcal{T}_{h,i}, \quad \mathcal{T}_{h,i}^\delta = \left\{ K \in \mathcal{T}_h : \exists K' \in \mathcal{T}_{h,i}^{\delta-1}, \partial K' \cap \partial K \neq \emptyset \right\}.$$

228 For each overlapping subdomain Ω_i^δ , the corresponding local finite element space is defined by

$$229 \quad \mathbf{V}_h^i = \left\{ \mathbf{v} \in V_h|_{\Omega_i^\delta} : \mathbf{v}|_{\partial\Omega_i^\delta \setminus (\partial\Omega \setminus \Gamma_w)} = 0 \right\}, \quad P_h^i = \left\{ q \in P_h|_{\Omega_i^\delta} : q|_{\partial\Omega_i^\delta \setminus \partial\Omega} = 0 \right\}.$$

230 Let $R_i : \mathbf{V}_h \times P_h \rightarrow \mathbf{V}_h^i \times P_h^i$ be a restriction operator which returns all degrees of freedom associated with
 231 the subspace $V_h^i \times P_h^i$ and the transpose R_i^T of R_i be the extension operator. Similarly we denote by R_i^0 as a
 232 restriction operator associated with the non-overlapping subdomains. Let A be the Jacobian matrix J_k^n and
 233 $A_i = R_i A R_i^T$ be the i th subdomain matrix. Then the one-level restricted additive Schwarz preconditioner
 234 [6] can be defined as

$$235 \quad (3.19) \quad M_{1s}^{-1} = \sum_{i=1}^{np} (R_i^0)^T A_i^{-1} R_i.$$

236 Finally, combining the coarse preconditioner (3.5) with the one-level preconditioner (3.19), we obtain the
 237 two-level additive Schwarz preconditioner

$$238 \quad (3.20) \quad M_{2s,cl}^{-1} = M_{cl}^{-1} + M_{1s}^{-1} = E_{cl} A_{cl}^{-1} R_{cl} + \sum_{i=1}^{np} (R_i^0)^T A_i^{-1} R_i.$$

239 In (3.20), the matrix A_{cl} derived from the discretization of the one-dimensional problem depends on the
 240 model parameter β . When $\beta = 0$, it means that the coarse problem is the one-dimensional Stokes problem
 241 and A_{cl} in Algorithm 3.1 stays unchanged for each time and Newton step. When $\beta = 1$, the one-dimensional
 242 problem represents a linearized unsteady incompressible Navier-Stokes problem and consequently A_{cl} needs
 243 to be recalculated at each time step based on the solution at the previous time step. In our implementation,
 244 for this case, u_h^{cl} at the previous time step is obtained by an interpolation of \mathbf{u}_h because the original one-
 245 dimensional problem (3.13) is not solved. Note that in (3.20) the coarse preconditioner and the one-level
 246 Schwarz preconditioner are added together; other hybrid versions [7, 61] can also be designed.

247 In this paper, we focus on the Newtonian model for the blood flows, the non-Newtonian effect is important
 248 for some situations [4, 22, 23, 29, 30, 39] and we expect that the extension of the proposed algorithm to
 249 non-Newtonian Navier-Stokes equations is straightforward [57].

250 **4. Numerical experiments.** In this section, we provide some numerical experiments to illustrate the
 251 effectiveness of the multiscale two-level restricted additive Schwarz preconditioner for unsteady incompress-
 252 ible Navier-Stokes flows in 3D patient-specific arteries. For the blood flows, we set the viscosity $\nu = 0.035$
 253 g/(cm·s), the density $\rho = 1$ g/cm³ and the source function $\mathbf{f} = 0$. On each outlet Γ_O^i , the resistance satisfies
 254 $R_i = R_{total} \left(\sum_{j=1}^m |\Gamma_O^j| / |\Gamma_O^i| \right)^{1.5}$ with a total resistance constant R_{total} to be given for each test case later [7].
 255 The BDF2 with $\Delta t = 0.005$ s is used for the temporal discretization and the stabilized $P_1 - P_1$ finite element
 256 method is used for the spatial discretization. At each time step, we solve the nonlinear system by an inexact
 257 Newton method with a line search technique. At each Newton step, the Jacobian system is solved by the
 258 right-preconditioned GMRES(30) method. The default parameters of Newton and GMRES stopping condi-
 259 tions in Algorithm 3.1 are $rtol_{Newton} = 10^{-4}$, $atol_{Newton} = 10^{-6}$ and $rtol_{GMRES} = 10^{-4}$, $atol_{GMRES} = 10^{-6}$.
 260 For the Schwarz preconditioners, we choose the overlapping parameter $\delta = 1$ and ILU with one fill-in level
 261 is used to solve the subdomain problems. In the experiments, we consider a tube and two patient-specific
 262 arteries with different 3D fine meshes (Table 1) and 1D coarse meshes (Table 2). For the one-dimensional
 263 coarse preconditioner, there are two models to use; i.e., the Stokes model ($\beta = 0$) and the Navier-Stokes
 264 model ($\beta = 1$). For the test problems considered in this paper, the Stokes model is quite efficient in terms
 265 of the number of GMRES iterations and the coarse preconditioner needs to be computed only once for all
 266 time steps and all Newton iterations (the subdomain matrices are recomputed at every Newton iteration),
 267 therefore in the following experiments, we use the Stokes model for most of the tests. In the end of the section
 268 we show some numerical results when the Navier-Stokes model is used. Note that in the following tables
 269 we only report the average number of GMRES iterations per Newton iteration and the average number of
 270 Newton iterations per time step is reported when the calculation is for a full cardiac cycle.

271 **4.1. Womersley flow in a tube.** We first verify the correctness of the implementation of the proposed
 272 algorithm by the Womersley flow in a tube with length $L_{tube} = 5$ cm and radius $R_{tube} = 0.5$ cm. It is known

Table 1: Details of three-dimensional fine meshes used in the experiments. N , E and h are the number of mesh points, the number of elements and the approximate mesh size, respectively.

Tube			Three-branch artery			Twelve-branch artery		
N	E	h (mm)	N	E	h (mm)	N	E	h (mm)
1789	8179	1.690	30114	147223	0.289	87866	380332	0.276
12542	65432	0.846	144701	752741	0.174	243013	1130531	0.188
93659	523456	0.422	1079408	6024816	0.087	1497225	8050242	0.100

Table 2: Details of one-dimensional coarse meshes used in the experiments. N_{cl} and h_{cl} are the number of mesh points and the approximate mesh size of the centerline, respectively.

Tube		Three-branch artery		Twelve-branch artery	
N_{cl}	h_{cl} (mm)	N_{cl}	h_{cl} (mm)	N_{cl}	h_{cl} (mm)
100	0.505	247	0.609	677	0.879

273 that (2.1) has the following analytic solution [20],

$$274 \quad u(r, t) = -\frac{R_{tube}^2}{\nu w_o^2} (\sin(t)J_1(r) + \cos(t)J_2(r)), v = 0, w = 0, p(x, t) = \cos(t) \left(x - \frac{L_{tube}}{2} \right),$$

275 where $r = \sqrt{y^2 + z^2}$, $w_o = R_{tube}\sqrt{\rho/\nu}$ is the Womersley number, $J_1(r)$, $J_2(r)$ are the real and imaginary
 276 parts of $J(r) = 1 - J_0(\Lambda \frac{r}{R_{tube}})J_0(\Lambda)^{-1}$, $\Lambda = w_o e^{i\frac{3}{4}\pi}$ with the zeroth order Bessel function of the first kind
 277 J_0 . For the boundary conditions, on the inlet the velocity is set to satisfy the exact velocity solution and on
 278 the outlet we set $R_{total} = 0$ dyn-s/cm⁵ to be consistent with the exact pressure solution. We compute the
 279 solution for a period of $[0, 2\pi]$ with $\Delta t = \pi/100$ and test three unstructured meshes described in Table 1. For
 280 this case, the maximum Reynolds number in a period is about 15. Fig. 5 shows the numerical results of the
 281 velocity profile, the distributions and the errors of the magnitude of the velocity and the average pressure
 282 difference between the inlet and the outlet. We can see that the numerical solutions gradually converge
 283 to the analytic solution with the use of finer meshes and the numerical solution with $N = 93659$ is quite
 284 close to the analytical solution, which indicates the correctness of the implementation. Table 3 shows the
 285 average number of Newton iterations at each time step and the average number of GMRES iterations at
 286 each Newton step with different preconditioners. The number of Newton iterations is almost independent of
 287 the fine mesh size, the coarse mesh size, the number of subdomains and the preconditioners, but the number
 288 of GMRES iterations is sensitive to the fine mesh size and the preconditioner. Compared with the one-level
 289 preconditioner, the new two-level preconditioner offers a better GMRES convergence and scalability with
 290 respect to the fine mesh size for this case.

291 **4.2. Patient-specific arteries.** In this subsection, we focus on two patient-specific arteries, including
 292 a three-branch artery and a twelve-branch artery. For the three-branch artery, there is one inlet with
 293 diameter 2.30 mm and three outlets with diameters 1.36 mm, 1.30 mm and 1.00 mm. For the twelve-branch
 294 artery, there is one inlet with diameter 3.00 mm and twelve outlets with diameters about 1.00 mm. On the
 295 inlet, we prescribe a pulsatile periodic flow velocity (see Fig. 6) with the parabolic profile. On the outlet,
 296 we set $R_{total} = 1500$ dyn-s/cm⁵. Three different unstructured meshes (see Table 1) for both arteries are
 297 considered. Note that the maximum Reynolds number is about 260 for the three-branch case and 340 for
 298 the twelve-branch case. For the two-level method, the coarse mesh information is given in Table 2.

299 First for the three-branch artery, we show the time histories of the velocity and pressure at different
 300 points for a cardiac cycle in Fig. 7. These curves of the velocity and pressure have the similar waveforms
 301 as the inlet flow waveform. Fig. 8 displays local features near the bifurcation at different phases. The
 302 velocity profiles have noticeable differences at the peak systole and early diastole phases. The maximum

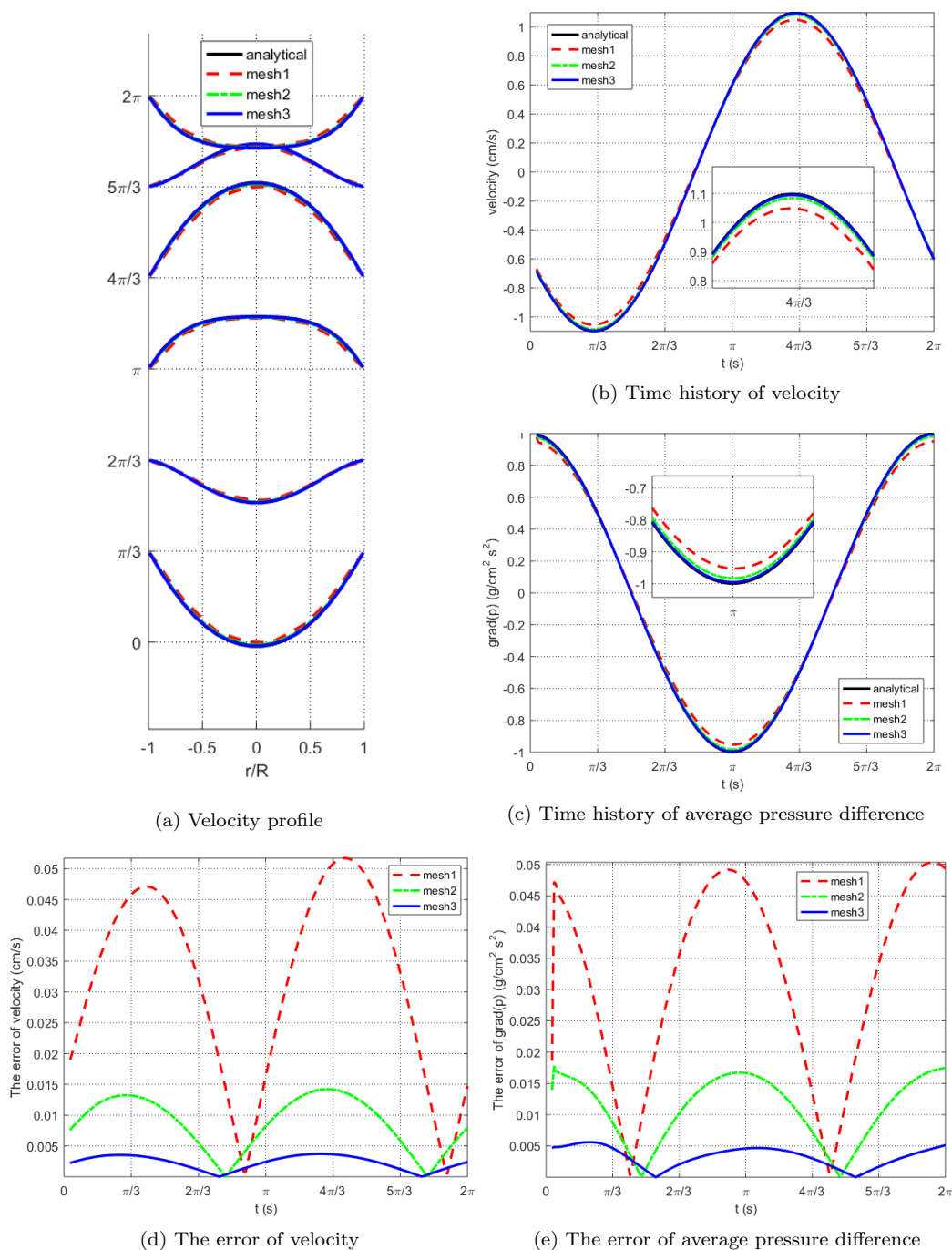


Fig. 5: A comparison of the analytical solution and the numerical solution obtained with three meshes with 1789, 12542 and 93659 mesh points labeled by ‘mesh1’, ‘mesh2’ and ‘mesh3’, respectively. (a): the velocity profile on the cross section $x = 0$ at different time $t = \pi/3, 2\pi/3, \pi, 4\pi/3, 5\pi/3, 2\pi$. (b): the time history of the velocity at the center $(0,0,0)$ of the tube. (c): the time history of the average pressure difference scaled by the length of the tube, i.e., the ratio of the pressure different between the inlet and the outlet and the length of the tube. (d): the error of the velocity shown in the subfigure (b). (e): the error of the average pressure difference shown in the subfigure (c). Note that the black solid line is covered by other lines.

Table 3: A comparison of the one-level and two-level preconditioners in terms of the average number of Newton iterations per time step and the average number of GMRES iterations per Newton iteration in a full period for the Womersley flow. N is the total number of mesh points, and np is the number of subdomains.

N	np	One-level		Two-level		
		Newton	GMRES	N_{cl}	Newton	GMRES
1789	8	1.74	12.06	34	1.84	5.74
12542	16	1.87	17.84	100	1.86	5.74
93659	32	1.88	29.43	100	1.84	6.46

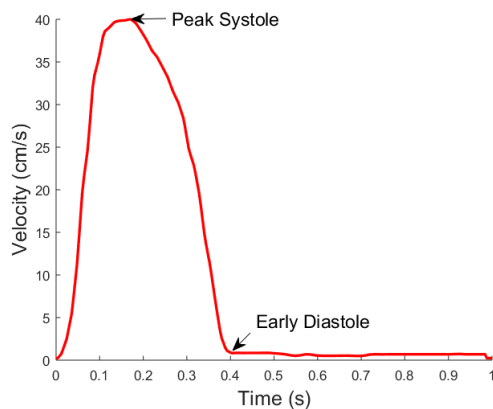


Fig. 6: The velocity pulse at the center of the inlet for a cardiac cycle.

303 value of the velocity magnitude happens in areas close to the wall and the corner of the bifurcation at the
 304 peak systole phase, but move to the internal center at the early diastole phase. The pressure at the corner
 305 of the bifurcation reaches the local maximum for both phases and the obvious vortex occurs at the early
 306 diastole. In Table 4 and 5, we give the number of Newton iterations and the average number of GMRES
 307 iterations at each Newton step of the one-level and two-level methods at the peak systole and the early
 308 diastole, respectively. Compared to the early diastole case, both methods require more GMRES
 309 iterations at the peak systole. For both phases, the two-level method scales much better with respect to the fine mesh
 310 size and the number of subdomains, but the one-level method performs poorly, especially on the fine mesh.

311 Further we consider the more complicated twelve-branch artery. Fig. 9 shows the magnitude of the
 312 velocity and the wall shear stress at different locations at the peak systole and the wall shear stress is defined
 313 by

$$314 \quad wss := -\nu \nabla \mathbf{u} \cdot \mathbf{n} + ((\nu \nabla \mathbf{u} \cdot \mathbf{n}) \cdot \mathbf{n}) \mathbf{n}.$$

315 Fig. 10 shows the streamlines at the peak systole. In order to study the effectiveness of the two-level method
 316 for this case, we provide the number of iterations at the peak systole (Table 6) and the early diastole (Table
 317 7) and observe similar behaviors as the three-branch case. Comparing the three-branch case with the twelve-
 318 branch case, for the one-level method, we see that the number of GMRES iterations increases a lot, but the
 319 increase of the two-level method is not much. These results indicate that the proposed two-level method is
 320 effective and robust with respect to the complexity of the arterial geometry.

321 The above discussions focus on the performance of the proposed method at two different times in a
 322 cardiac cycle, namely the peak systole phase when the velocity and pressure are near their maximum values
 323 and the early diastole phase when their respective values are close to their minimum. In Table 8 we illustrate
 324 the performance in a complete cardiac cycle. The average number of Newton iterations stays unchanged
 325 and the average number of GMRES iterations has a small increase when refining the mesh, and we can

Table 4: At the systole phase: a comparison of one-level and two-level preconditioners in terms of the number of iterations for the three-branch artery. N is the total number of mesh points, and np is the number of subdomains.

Phase	N	np	One-level		Two-level		
			Newton	GMRES	Newton	GMRES	
Systole	30114	16	2	297.50	2	19.50	
		32	2	307.50	2	19.50	
		64	2	319.50	2	20.00	
	144701	32	2	583.50	2	24.50	
		64	2	558.00	2	25.00	
		128	2	633.50	2	24.00	
		256	2	485.00	2	36.00	
		1079408	512	2	807.50	2	36.00
			1024	2	1128.50	2	36.50

Table 5: At the diastole phase: a comparison of one-level and two-level preconditioners in terms of the number of iterations for the three-branch artery. N is the total number of mesh points, and np is the number of subdomains.

Phase	N	np	One-level		Two-level		
			Newton	GMRES	Newton	GMRES	
Diastole	30114	16	2	156.50	2	15.00	
		32	2	134.00	2	15.00	
		64	2	247.00	2	15.00	
	144701	32	2	226.50	2	17.00	
		64	2	222.50	2	17.50	
		128	2	235.50	2	17.00	
		256	2	244.50	2	25.00	
		1079408	512	2	366.50	2	25.50
			1024	2	426.50	2	25.50

Table 6: At the systole phase: a comparison of one-level and two-level preconditioners in terms of the number of iterations for the twelve-branch artery. N is the total number of mesh points, and np is the number of subdomains.

Phase	N	np	One-level		Two-level	
			Newton	GMRES	Newton	GMRES
Systole	87866	32	2	675.00	2	36.00
		64	2	748.50	2	36.50
		128	2	845.50	2	36.00
	243013	64	2	1318.50	2	41.00
		128	2	980.50	2	41.00
		256	2	1214.50	2	42.00
		256	4	2670.00	2	113.00
	1497225	512	3	2461.00	2	113.00
		1024	3	2841.33	2	112.00

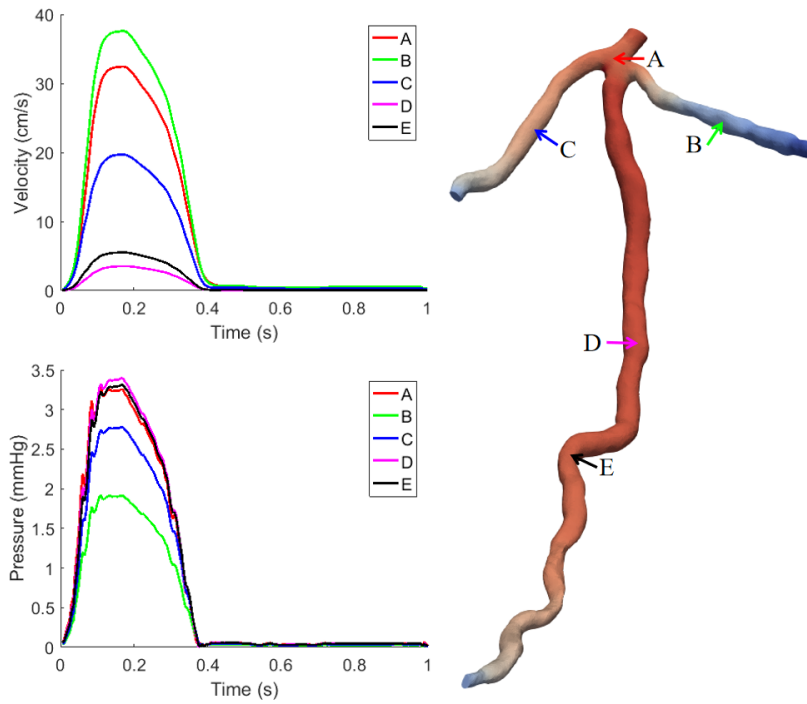


Fig. 7: The time histories of the velocity and pressure at different points for a cardiac cycle.

Table 7: At the diastole phase: a comparison of one-level and two-level preconditioners in terms of the number of iterations for the twelve-branch artery. N is the total number of mesh points, and np is the number of subdomains.

Phase	N	np	One-level		Two-level	
			Newton	GMRES	Newton	GMRES
Diastole	87866	32	2	279.00	2	26.00
		64	2	280.00	2	25.50
		128	2	328.00	2	26.50
		64	2	412.00	2	26.50
	243013	128	2	425.00	2	26.50
		256	2	463.00	2	27.00
		256	2	651.50	2	62.50
		1497225	512	2	655.00	2
1024	2		890.50	2	63.00	

326 see that the two-level method works well for the full cardiac cycle. Next, we consider the impact of other
 327 algorithmic parameters including the ILU fill-in level, the overlapping parameter and the coarse mesh size.
 328 Table 9 shows the number of iterations for different ILU fill-in levels and indicates that the ILU fill-in level
 329 has an obvious impact on the number of GMRES iterations and ILU(2) can clearly improve the GMRES
 330 convergence. Considering the overlapping parameter, Table 10 shows that a small overlapping parameter is
 331 enough, which is consistent with the classical theory of two-level Schwarz methods in [13]. Table 11 lists the
 332 number of iterations with different coarse meshes and shows, as expected, that a finer coarse mesh provides
 333 a better GMRES convergence especially at the systole phase of a cardiac cycle.

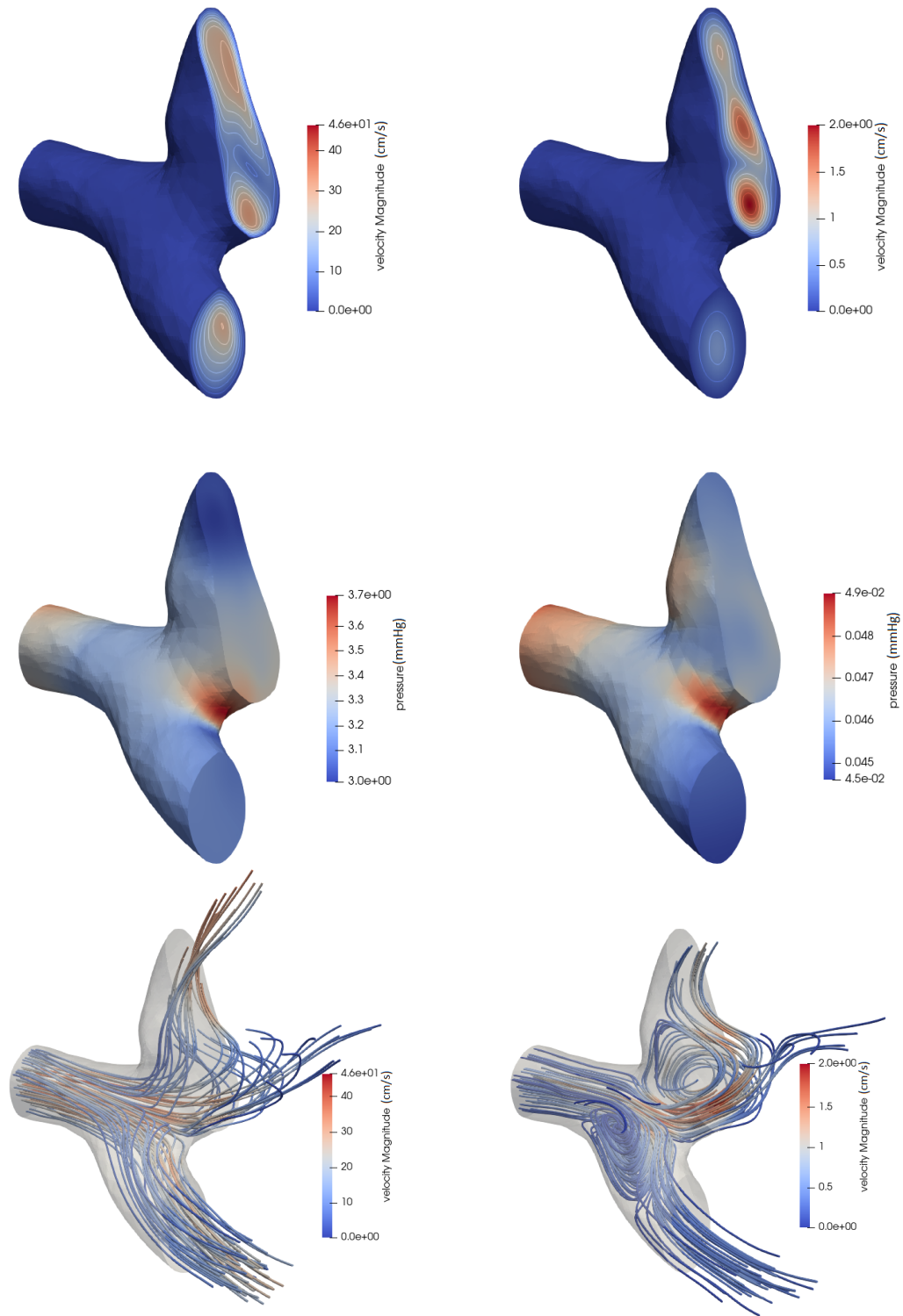


Fig. 8: The distributions of the magnitude of the velocity (top), pressure (middle) and the streamline (bottom) near the bifurcation at the systole phase when $t = 0.165$ s (left) and the diastole phase when $t = 0.405$ s (right).

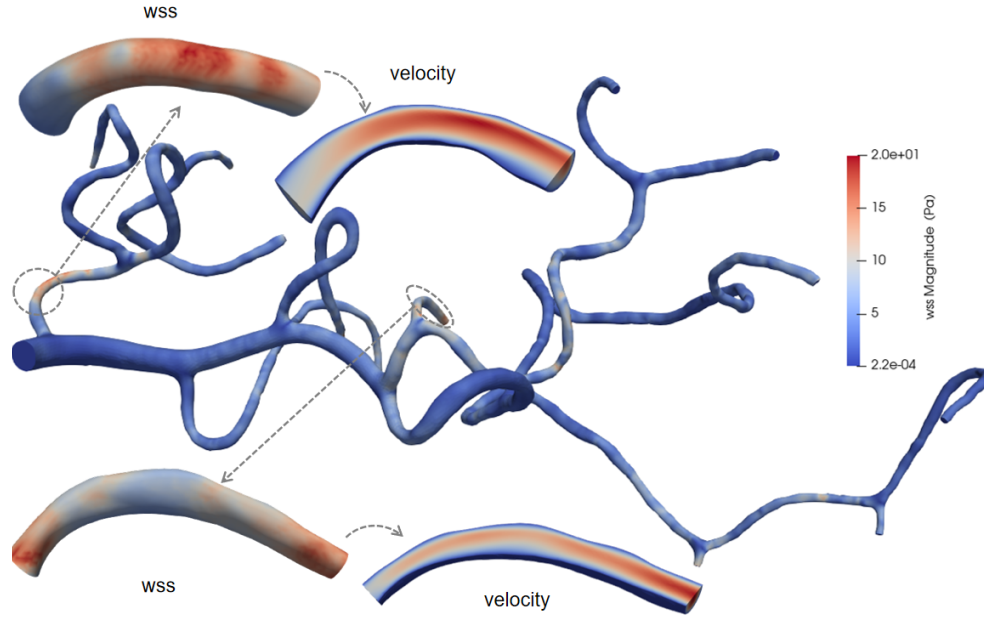


Fig. 9: The wall shear stress and velocity magnitude at different locations at the peak systole.

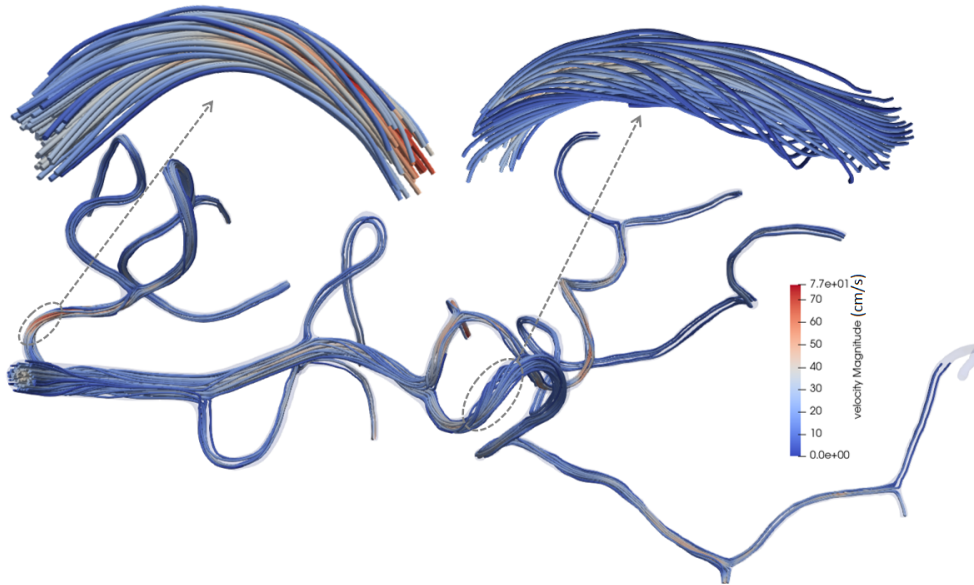


Fig. 10: The streamlines at different locations at the peak systole.

334 Next, in Table 12, we present the performance of the one-dimensional coarse preconditioner for different
 335 time step sizes when there is a stenosis in the artery. In this experiment, we test the three-branch artery
 336 with and without a stenosis which reduces the diameter of the artery by 50%, as shown in Fig. 11. Fig. 11
 337 also shows the distribution of the pressure which decreases rapidly passing the stenosis. Table 12 indicates
 338 that with the increase of the time step size, the numbers of Newton and GMRES iterations both increase
 339 slightly.

Table 8: The average number of iterations of the two-level preconditioner in a cardiac cycle for three-branch and twelve-branch arteries. N is the total number of mesh points, and np is the number of subdomains.

Artery	N	np	Newton	GMRES
Three-branch	30114	16	1.59	16.70
	144701	32	1.58	18.56
	1079408	256	1.53	28.43
Twelve-branch	87866	32	1.70	33.33
	243013	64	1.69	33.68
	1497225	256	1.66	71.27

Table 9: The effect of the ILU fill-in level ‘ILU’ on the number of iterations of the two-level preconditioner.

Phase	ILU	Three-branch		Twelve-branch	
		Newton	GMRES	Newton	GMRES
Systole	0	2	62.00	2	234.00
	1	2	36.00	2	113.00
	2	2	29.50	2	72.00
Diastole	0	2	36.50	2	95.50
	1	2	25.00	2	62.50
	2	2	20.00	2	43.00

340 Note that the coarse preconditioner in all the experiments presented so far in this section is constructed
341 based on the one-dimensional Stokes model ($\beta = 0$). In order to show the effect of the one-dimensional Navier-
342 Stokes model ($\beta = 1$) on the number of iterations, in Table 13, we provide a comparison of the number of
343 iterations with different coarse models for the twelve-branch artery. We see that the one-dimensional Navier-
344 Stokes model moderately improves the GMRES convergence at the peak systole and the difference is quite
345 small at the early diastole. Therefore we conclude that for problems considered in this paper, the Stokes
346 model is sufficient, but for more complicated problems the Navier-Stokes model might be more useful.

347 **5. Conclusions.** Modeling blood flows using the three-dimensional unsteady incompressible Navier-
348 Stokes equations in patient-specific arteries with many bifurcating branches is computationally very expen-
349 sive. In this paper, we developed a Newton-Krylov method with an effective two-level restricted additive
350 Schwarz preconditioner consisting of overlapping three-dimensional subdomain preconditioners and a one-
351 dimensional coarse preconditioner constructed by a parameterized unsteady Navier-Stokes model defined on
352 the centerline of the artery with appropriate 3D-1D restriction and 1D-3D extension operators. The key
353 feature of the method is that the cost of the one-dimensional coarse problem is almost neglectable but it
354 reduces significantly the number of GMRES iterations comparing with the one-level method. Numerical
355 experiments show that the proposed method is not only scalable in terms of the numbers of linear and
356 nonlinear iterations, but is also quite robust with respect to the complex geometry of the artery and varying
357 flow conditions. In the future work, we plan to further develop the method for diseased arteries with, for
358 example, aneurysm or stenosis, as well as study its performance on large-scale parallel computers.

359

REFERENCES

- 360 [1] M. S. ALNÆS, J. ISAKSEN, K.-A. MARDAL, B. RØMNER, M. K. MORGAN, AND T. INGEBRIGTSEN, *Computation of hemo-*
361 *dynamics in the circle of Willis*, *Stroke*, 38 (2007), pp. 2500–2505.
362 [2] D. BALZANI, D. BÖSE, D. BRANDS, R. ERBEL, A. KLAWONN, O. RHEINBACH, AND J. SCHRÖDER, *Parallel simulation of*
363 *patient-specific atherosclerotic arteries for the enhancement of intravascular ultrasound diagnostics*, *Engrg. Comput.*,
364 (2012).
365 [3] A. T. BARKER AND X.-C. CAI, *Scalable parallel methods for monolithic coupling in fluid-structure interaction with*

Table 10: The effect of the overlapping parameter δ on the number of iterations of two-level preconditioners.

Phase	δ	Three-branch		Twelve-branch	
		Newton	GMRES	Newton	GMRES
Systole	1	2	36.00	2	113.00
	2	2	35.00	2	104.00
	3	2	34.00	2	100.50
Diastole	1	2	25.00	2	62.50
	2	2	24.00	2	63.00
	3	2	22.50	2	63.00

Table 11: The effect of the number of coarse mesh points N_{cl} on the number of iterations of two-level preconditioners.

Phase	Three-branch			Twelve-branch		
	N_{cl}	Newton	GMRES	N_{cl}	Newton	GMRES
Systole	88	2	53.50	522	2	128.00
	128	2	46.50	677	2	113.00
	247	2	36.00	998	2	99.00
Diastole	88	2	38.00	522	2	64.00
	128	2	32.50	677	2	62.50
	247	2	25.00	998	2	61.00

Table 12: The performance of the one-dimensional coarse preconditioner with respect to the time step size and the three-branch artery with and without a stenosis at $t = 0.16$ s. N is the total number of mesh points.

Geometry	N	Δt (s)	Newton	GMRES
Norm	331370	0.005	2	30.00
		0.01	2	41.50
		0.02	3	46.00
Stenosis	329938	0.005	2	30.50
		0.01	2	44.50
		0.02	3	48.00

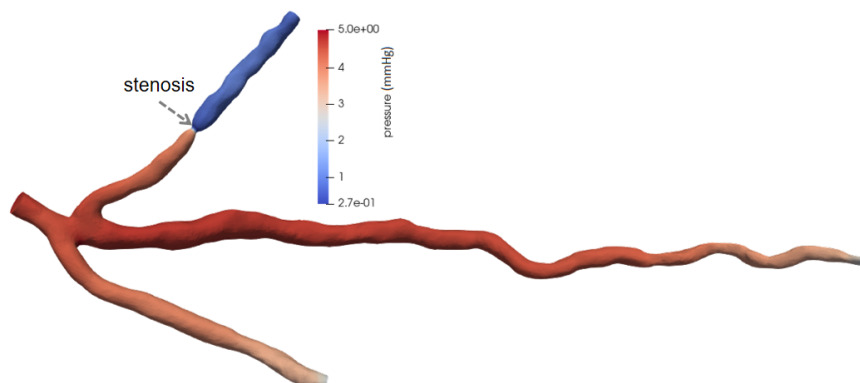
Fig. 11: The distribution of the pressure at $t = 0.16$ s for the three-branch artery with a stenosis.

Table 13: A comparison of the coarse preconditioner with one-dimensional Stokes ($\beta = 0$) and Navier-Stokes ($\beta = 1$) models in terms of the number of iterations. $rtol_{\text{GMRES}}$ is the GMRES relative tolerance.

Phase	$rtol_{\text{GMRES}}$	$\beta = 0$		$\beta = 1$	
		Newton	GMRES	Newton	GMRES
Systole	10^{-4}	2	113.00	2	89.50
	10^{-3}	2	94.00	2	77.50
	10^{-2}	2	85.00	2	78.00
Diastole	10^{-4}	2	62.50	2	63.00
	10^{-3}	2	45.00	2	45.00
	10^{-2}	2	36.00	2	36.00

- 366 *application to blood flow modeling*, J. Comput. Phys., 229 (2010), pp. 642–659.
- 367 [4] J. BERNSDORF AND D. WANG, *Non-Newtonian blood flow simulation in cerebral aneurysms*, Comput. Math. Appl., 58
- 368 (2009), pp. 1024–1029.
- 369 [5] X.-C. CAI, W. D. GROPP, D. E. KEYES, R. G. MELVIN, AND D. P. YOUNG, *Parallel Newton-Krylov-Schwarz algorithms*
- 370 *for the transonic full potential equation*, SIAM J. Sci. Comput., 19 (1998), pp. 246–265.
- 371 [6] X.-C. CAI AND M. SARKIS, *A restricted additive Schwarz preconditioner for general sparse linear systems*, SIAM J. Sci.
- 372 Comput., 21 (1999), pp. 792–797.
- 373 [7] R. CHEN, B. WU, Z. CHENG, W.-S. SHIU, J. LIU, L. LIU, Y. WANG, X. WANG, AND X.-C. CAI, *A parallel non-nested*
- 374 *two-level domain decomposition method for simulating blood flows in cerebral artery of stroke patient*, Int. J. Numer.
- 375 Methods Biomed. Eng., 36 (2020), p. e3392.
- 376 [8] J. S. COOGAN, J. D. HUMPHREY, AND C. A. FIGUEROA, *Computational simulations of hemodynamic changes within*
- 377 *thoracic, coronary, and cerebral arteries following early wall remodeling in response to distal aortic coarctation*,
- 378 Biomech. Model. Mechanobiol., 12 (2013), pp. 79–93.
- 379 [9] J. E. DENNIS, JR. AND R. B. SCHNABEL, *Numerical Methods for Unconstrained Optimization and Nonlinear Equations*,
- 380 SIAM, Philadelphia, PA, 1996.
- 381 [10] S. DEPARIS, D. FORTI, G. GRANDPERRIN, AND A. QUARTERONI, *FaCSI: a block parallel preconditioner for fluid-structure*
- 382 *interaction in hemodynamics*, J. Comput. Phys., 327 (2016), pp. 700–718.
- 383 [11] S. DEPARIS, G. GRANDPERRIN, AND A. QUARTERONI, *Parallel preconditioners for the unsteady Navier-Stokes equations*
- 384 *and applications to hemodynamics simulations*, Comput. & Fluids, 92 (2014), pp. 253–273.
- 385 [12] C. R. DOHRMANN, A. KLAWONN, AND O. B. WIDLUND, *Domain decomposition for less regular subdomains: overlapping*
- 386 *Schwarz in two dimensions*, SIAM J. Numer. Anal., 46 (2008), pp. 2153–2168.
- 387 [13] M. DRYJA AND O. B. WIDLUND, *Domain decomposition algorithms with small overlap*, SIAM J. Sci. Comput., 15 (1994),
- 388 pp. 604–620.
- 389 [14] H. ELMAN, V. E. HOWLE, J. SHADID, R. SHUTTLEWORTH, AND R. TUMINARO, *A taxonomy and comparison of parallel block*
- 390 *multi-level preconditioners for the incompressible Navier-Stokes equations*, J. Comput. Phys., 227 (2008), pp. 1790–
- 391 1808.
- 392 [15] C. FISHER AND J. S. ROSSMANN, *Effect of non-Newtonian behavior on hemodynamics of cerebral aneurysms*, J. Biomech.
- 393 Eng., 131 (2009).
- 394 [16] L. FORMAGGIA, J.-F. GERBEAU, F. NOBILE, AND A. QUARTERONI, *On the coupling of 3D and 1D Navier–Stokes equations*
- 395 *for flow problems in compliant vessels*, Comput. Methods Appl. Mech. Engrg., 191 (2001), pp. 561–582.
- 396 [17] L. FORMAGGIA, D. LAMPONI, AND A. QUARTERONI, *One-dimensional models for blood flow in arteries*, J. Engrg. Math.,
- 397 47 (2003), pp. 251–276.
- 398 [18] L. FORMAGGIA, F. NOBILE, A. QUARTERONI, AND A. VENEZIANI, *Multiscale modelling of the circulatory system: a pre-*
- 399 *liminary analysis*, Comput. Vis. Sci., 2 (1999), pp. 75–83.
- 400 [19] L. P. FRANCA AND S. L. FREY, *Stabilized finite element methods. II. The incompressible Navier-Stokes equations*, Comput.
- 401 Methods Appl. Mech. Engrg., 99 (1992), pp. 209–233.
- 402 [20] Y. C. FUNG, *Biomechanics: Motion, Flow, Stress, and Growth*, Springer-Verlag, 1990.
- 403 [21] M. W. GEE, U. KÜTTLER, AND W. A. WALL, *Truly monolithic algebraic multigrid for fluid-structure interaction*, Int. J.
- 404 Numer. Methods Engrg., 85 (2011), pp. 987–1016.
- 405 [22] F. GIJSEN, E. ALLANIC, F. VAN DE VOSSE, AND J. JANSSEN, *The influence of the non-Newtonian properties of blood on*
- 406 *the flow in large arteries: unsteady flow in a 90 curved tube*, J. Biomech., 32 (1999), pp. 705–713.
- 407 [23] F. J. GIJSEN, F. N. VAN DE VOSSE, AND J. JANSSEN, *The influence of the non-Newtonian properties of blood on the flow*
- 408 *in large arteries: steady flow in a carotid bifurcation model*, J. Biomech., 32 (1999), pp. 601–608.
- 409 [24] L. GRINBERG, E. CHEEVER, T. ANOR, J. R. MADSEN, AND G. KARNIADAKIS, *Modeling blood flow circulation in intracranial*
- 410 *arterial networks: a comparative 3D/1D simulation study*, Ann. Biomed. Eng., 39 (2011), pp. 297–309.
- 411 [25] L. GRINBERG, D. A. FEDOSOV, AND G. E. KARNIADAKIS, *Parallel multiscale simulations of a brain aneurysm*, J. Comput.
- 412 Phys., 244 (2013), pp. 131–147.
- 413 [26] J. L. GUERMOND, P. MINEV, AND J. SHEN, *An overview of projection methods for incompressible flows*, Comput. Methods
- 414 Appl. Mech. Engrg., 195 (2006), pp. 6011–6045.

- 415 [27] A. HEINLEIN, C. HOCHMUTH, AND A. KLAWONN, *Monolithic overlapping Schwarz domain decomposition methods with*
 416 *GDSW coarse spaces for incompressible fluid flow problems*, SIAM J. Sci. Comput., 41 (2019), pp. C291–C316.
- 417 [28] A. HEINLEIN, C. HOCHMUTH, AND A. KLAWONN, *Reduced dimension GDSW coarse spaces for monolithic Schwarz domain*
 418 *decomposition methods for incompressible fluid flow problems*, Internat. J. Numer. Methods Engrg., 121 (2020),
 419 pp. 1101–1119.
- 420 [29] B. M. JOHNSTON, P. R. JOHNSTON, S. CORNEY, AND D. KILPATRICK, *Non-Newtonian blood flow in human right coronary*
 421 *arteries: steady state simulations*, J. Biomech., 37 (2004), pp. 709–720.
- 422 [30] B. M. JOHNSTON, P. R. JOHNSTON, S. CORNEY, AND D. KILPATRICK, *Non-Newtonian blood flow in human right coronary*
 423 *arteries: transient simulations*, J. Biomech., 39 (2006), pp. 1116–1128.
- 424 [31] G. KARYPIS AND V. KUMAR, *Multilevelk-way partitioning scheme for irregular graphs*, J. Parallel Distrib. Comput., 48
 425 (1998), pp. 96–129.
- 426 [32] A. KLAWONN, *An optimal preconditioner for a class of saddle point problems with a penalty term*, SIAM J. Sci. Comput.,
 427 19 (1998), pp. 540–552.
- 428 [33] A. KLAWONN, *Block-triangular preconditioners for saddle point problems with a penalty term*, SIAM J. Sci. Comput., 19
 429 (1998), pp. 172–184.
- 430 [34] A. KLAWONN AND L. F. PAVARINO, *Overlapping Schwarz methods for mixed linear elasticity and Stokes problems*, Comput.
 431 Methods Appl. Mech. Engrg., 165 (1998), pp. 233–245.
- 432 [35] D. A. KNOLL AND D. E. KEYES, *Jacobian-free Newton-Krylov methods: a survey of approaches and applications*, J.
 433 Comput. Phys., 193 (2004), pp. 357–397.
- 434 [36] D. A. KNOLL AND W. J. RIDER, *A multigrid preconditioned Newton-Krylov method*, SIAM J. Sci. Comput., 21 (1999),
 435 pp. 691–710.
- 436 [37] F. KONG AND X.-C. CAI, *A highly scalable multilevel Schwarz method with boundary geometry preserving coarse spaces*
 437 *for 3D elasticity problems on domains with complex geometry*, SIAM J. Sci. Comput., 38 (2016), pp. C73–C95.
- 438 [38] F. KONG AND X.-C. CAI, *A scalable nonlinear fluid–structure interaction solver based on a Schwarz preconditioner with*
 439 *isogeometric unstructured coarse spaces in 3D*, J. Comput. Phys., 340 (2017), pp. 498–518.
- 440 [39] J. LEE AND N. SMITH, *Development and application of a one-dimensional blood flow model for microvascular networks*,
 441 Proc. Inst. Mech. Eng. H: J. Eng. Med., 222 (2008), pp. 487–511.
- 442 [40] J. LI AND O. WIDLUND, *BDDC algorithms for incompressible Stokes equations*, SIAM J. Numer. Anal., 44 (2006), pp. 2432–
 443 2455.
- 444 [41] Z. LIN, R. CHEN, B. GAO, S. QIN, B. WU, J. LIU, AND X.-C. CAI, *A highly parallel simulation of patient-specific hepatic*
 445 *flows*, Int. J. Numer. Methods Biomed. Eng., 37 (2021), p. e3451.
- 446 [42] Y. LIU AND X.-C. CAI, *A central-line coarse preconditioner for Stokes flows in artery-like domains*, Numer. Algorithms,
 447 87 (2021), pp. 137–160.
- 448 [43] J. M. MURABITO, R. B. D’AGOSTINO, H. SILBERSHATZ, AND P. W. WILSON, *Intermittent claudication: a risk profile from*
 449 *the Framingham Heart Study*, Circulation, 96 (1997), pp. 44–49.
- 450 [44] S. QIN, B. WU, J. LIU, W.-S. SHIU, Z. YAN, R. CHEN, AND X.-C. CAI, *Efficient parallel simulation of hemodynamics in*
 451 *patient-specific abdominal aorta with aneurysm*, Comput. Biol. Med., 136 (2021), p. 104652.
- 452 [45] S. QIN, B. WU, J. LIU, W.-S. SHIU, Z. YAN, R. CHEN, AND X.-C. CAI, *Numerical simulation of blood flows in patient-*
 453 *specific abdominal aorta with primary organs*, Biomech. Model. Mechanobiol., 20 (2021), pp. 909–924.
- 454 [46] A. QUARTERONI AND L. FORMAGGIA, *Mathematical modelling and numerical simulation of the cardiovascular system*,
 455 Handbook of Numerical Analysis, 12 (2004), pp. 3–127.
- 456 [47] A. QUARTERONI, A. MANZONI, AND C. VERGARA, *The cardiovascular system: mathematical modelling, numerical algo-*
 457 *rithms and clinical applications*, Acta Numer., 26 (2017), pp. 365–590.
- 458 [48] A. QUARTERONI, F. SALERI, AND A. VENEZIANI, *Analysis of the Yosida method for the incompressible Navier-Stokes*
 459 *equations*, J. Math. Pures Appl. (9), 78 (1999), pp. 473–503.
- 460 [49] A. QUARTERONI, F. SALERI, AND A. VENEZIANI, *Factorization methods for the numerical approximation of Navier-Stokes*
 461 *equations*, Comput. Methods Appl. Mech. Engrg., 188 (2000), pp. 505–526.
- 462 [50] A. QUARTERONI, M. TUVERI, AND A. VENEZIANI, *Computational vascular fluid dynamics: problems, models and methods*,
 463 Comput. Vis. Sci., 2 (2000), pp. 163–197.
- 464 [51] A. RANGLES, E. W. DRAEGER, T. OPPELSTRUP, L. KRAUSS, AND J. A. GUNNELS, *Massively parallel models of the human*
 465 *circulatory system*, in Proceedings of the International Conference for High Performance Computing, Networking,
 466 Storage and Analysis, SC ’15, New York, NY, USA, 2015, Association for Computing Machinery, pp. 1–11.
- 467 [52] P. REYMOND, F. MERENDA, F. PERREN, D. RUFENACHT, AND N. STERGIOPULOS, *Validation of a one-dimensional model*
 468 *of the systemic arterial tree*, Am. J. Physiol. - Heart Circ. Physiol., 297 (2009), pp. H208–H222.
- 469 [53] P. REYMOND, F. PERREN, F. LAZEYRAS, AND N. STERGIOPULOS, *Patient-specific mean pressure drop in the systemic*
 470 *arterial tree, a comparison between 1-D and 3-D models*, J. Biomech., 45 (2012), pp. 2499–2505.
- 471 [54] Y. SAAD, *Iterative Method for Sparse Linear Systems*, SIAM, Philadelphia, PA, second ed., 2003.
- 472 [55] D. M. SFORZA, C. M. PUTMAN, AND J. R. CEBRAL, *Hemodynamics of cerebral aneurysms*, Annu. Rev. Fluid Mech., 41
 473 (2009), pp. 91–107.
- 474 [56] S. SHERWIN, V. FRANKE, J. PEIRO, AND K. PARKER, *One-dimensional modelling of a vascular network in space-time*
 475 *variables*, J. Engrg. Math., 47 (2003), pp. 217–250.
- 476 [57] W.-S. SHIU, F.-N. HWANG, AND X.-C. CAI, *Parallel domain decomposition method for finite element approximation of*
 477 *3D steady state non-Newtonian fluids*, Internat. J. Numer. Methods Fluids, 78 (2015), pp. 502–520.
- 478 [58] N. SMITH, A. PULLAN, AND P. HUNTER, *An anatomically based model of transient coronary blood flow in the heart*, SIAM
 479 J. Appl. Math., 62 (2002), pp. 990–1018.
- 480 [59] C. A. TAYLOR, T. J. HUGHES, AND C. K. ZARINS, *Finite element modeling of blood flow in arteries*, Comput. Methods
 481 Appl. Mech. Engrg., 158 (1998), pp. 155–196.
- 482 [60] C. A. TAYLOR AND J. D. HUMPHREY, *Open problems in computational vascular biomechanics: hemodynamics and arterial*

- 483 *wall mechanics*, *Comput. Methods Appl. Mech. Engrg.*, 198 (2009), pp. 3514–3523.
- 484 [61] A. TOSELLI AND O. WIDLUND, *Domain Decomposition Methods—Algorithms and Theory*, Springer-Verlag, Berlin, 2005.
- 485 [62] I. E. VIGNON-CLEMENTEL, C. A. FIGUEROA, K. E. JANSEN, AND C. A. TAYLOR, *Outflow boundary conditions for three-*
- 486 *dimensional finite element modeling of blood flow and pressure in arteries*, *Comput. Methods Appl. Mech. Engrg.*,
- 487 195 (2006), pp. 3776–3796.
- 488 [63] Y. ZHANG, Y. BAZILEVS, S. GOSWAMI, C. L. BAJAJ, AND T. J. HUGHES, *Patient-specific vascular NURBS modeling for*
- 489 *isogeometric analysis of blood flow*, *Comput. Methods Appl. Mech. Engrg.*, 196 (2007), pp. 2943–2959.